Journal of Sound and Vibration (2002) **251**(3), 431–456
doi:10.1006/jsvi.2001.4009, available online at http://www.idealibrary.com on IDEAL®

SOUND TRANSMISSION THROUGH PERIODICALLY STIFFENED CYLINDRICAL SHELLS

J.-H. Lee and J. Kim

Structural Dynamics Research Laboratory, Mechanical Engineering Department, University of Cincinnati, Cincinnati, OH 45221-0072, *U.S.A.*
E-mail: jay.kim@uc.edu

(*Received* 26 *February* 2001, *and in final form* 4 *September* 2001)

A relatively long circular cylindrical shell stiffened by periodically deployed stiffeners is found in many practical applications such as the aircraft fuselage. For the sound transmission analysis of such a system, not only structural interactions between the shell and stiffeners but also vibro-acoustic interactions between the structure and acoustic media have to be considered. By idealizing the system as an infinitely long cylinder subjected to a plane wave incidence, an exact solution is obtained for the first time for this type of problem. In the analysis, the solution is obtained in a series form by expanding the system responses in terms of the space harmonics of the stiffener spacing. Characteristics of the system responses and effects of important design parameters are studied using the transmission losses calculated from the analysis.

1. INTRODUCTION

Cylindrical shells stiffened by periodically deployed stiffeners are found in many practical systems of interest such as in the aircraft fuselage or marine structures. Analysis of such a system for sound transmission calculation becomes very complicated because of the presence of stiffeners and the need to model structural, and structure–acoustic coupling effects. Mead *et al.* [1–3] solved free and forced vibration problems of flat panels with periodic stiffeners using the space harmonic method. In their work, responses of the structure to acoustic excitations were obtained by ignoring the effect of the structural response on the acoustic system. The analysis necessary to calculate the sound transmission through a stiffened structure becomes more complicated because the interactions between the structure and acoustic media have to be included in the system analysis. Analytical or numerical studies are found on the structural responses of periodically stiffened structures [4–9], and periodically stiffened cylindrical shells [10–22], or sound transmissions through cylindrical shells [23–26]; however, no reported work is found that obtained analytical solutions for the sound transmission through stiffened shells.

Mead and his collaborators [1–3, 7] investigated the structural responses of periodically stiffened structures by superposing travelling wave solutions described in terms of the harmonics of each period of the stiffened structures, which were called the space harmonics [2]. They studied characteristics of the free and forced vibration responses of the periodically stiffened structures to the convective acoustic pressure field. This space harmonics method is adopted in this work to model the structural part of the system.

Structural responses of stiffened cylindrical shells are studied by some researchers, mostly by numerical methods. Mecitoğlu and his colleagues [11] studied free vibrations of a stiffened shallow shell using an approach within the frame of Love's equation for elastic

0022-460X/02/130431 + 26 $35.00/0

shells and also by using the finite element method [12]. He also studied free vibration problems by using a simplified shell theory within the context of *Donnell–Mushtari theory* [13]. Egle and Sewall [14] studied the vibration of orthogonally stiffened cylindrical shells with discrete axial stiffeners by using the Ritz method. Bushnell [15] compared various analytical models to analyze vibration problems of stiffened shells. Mead and Bardell [16] studied free vibrations of a thin cylindrical shell with discrete axial and circumferential stiffeners. Mustafa and Ali [17, 18] determined the frequencies of ring stiffened, stringer stiffened and orthogonally stiffened shells by using super shell finite elements. Sivasubramonian *et al.* [19] studied the free vibration characteristics of a longitudinally stiffened curved panel by using the finite element method. Lam and Hua [20] investigated the influence of boundary conditions on the frequency characteristics of a rotating conical shell by using the Galerkin method. Markuš and Mead [21, 22] presented the study on harmonic wave propagation in thick circular orthotropic cylinders and a three-layered composite thick cylinder, which was carried out within the framework of the complete three-dimensional theory of elasticity by using Bessel and special Frobenius series.

Sound transmissions through various types of cylindrical shells, which however were not stiffened, have been studied by many investigators [23–36] including the authors [33–36]. In the authors' previous studies, exact solutions were obtained for the sound transmissions through cylindrical shells of various cross-sectional structures including a single-walled shell [33], double-walled shell [34], and double-walled shells with a core of porous layer [35]. In this study, the basic modelling and analysis schemes to consider the structure–acoustic coupling effect are adopted from the authors' previous studies [33–36], while the space harmonic expansion method developed by Mead *et al.* [2] is employed to model the effects of periodic stiffeners.

2. FORMULATION OF THE SYSTEM EQUATION

A schematic illustration is shown for a cylindrical shell with periodically deployed stiffeners in one direction (z direction in this case) in Figure 1. The system is simplified by three assumptions that have been typically used to calculate the transmission losses (TLs) of relatively long cylindrical structures [23–36], which are that the cylinder is infinitely long, the input wave is a plane wave travelling on the plane parallel to the x–z plane with an incidence angle γ, and the inside cavity is anechoic. This model approximates the sound transmission problem into the aircraft cabin [25–31] or the reciprocal of the sound transmission from the hermetic cylindrical machineries running in the anechoic chamber [36]. As shown in Figure 1, the stiffener is modelled by a combination of the lumped mass M, translational spring K_t and rotational spring K_r. Either experimental or numerical methods, may be used to find these spring rates. For example, an FE analysis may be used to find the ratios of the vertical force and displacement and the angular moment and displacement that may be used as the spring rates. The shell is characterized by its radius R, wall thickness h, *in vacuo* bulk mass density ρ_s, *in vacuo* bulk Young's modulus E_s and the Poisson ratio μ_s. The acoustic media on the outside and the inside of the shell are defined by the density and speed of sound: $\{\rho_1, c_1\}$ inside and $\{\rho_2, c_2\}$ outside. Since the structure is spatially periodic, the virtual work done by only one bay element (including supports) needs to be considered.

2.1. ASSUMED SOLUTIONS

Considering the periodic nature of the structure [1–3] and the assumed mode of the cylindrical shell [37], the shell displacements can be expressed in terms of a series of space

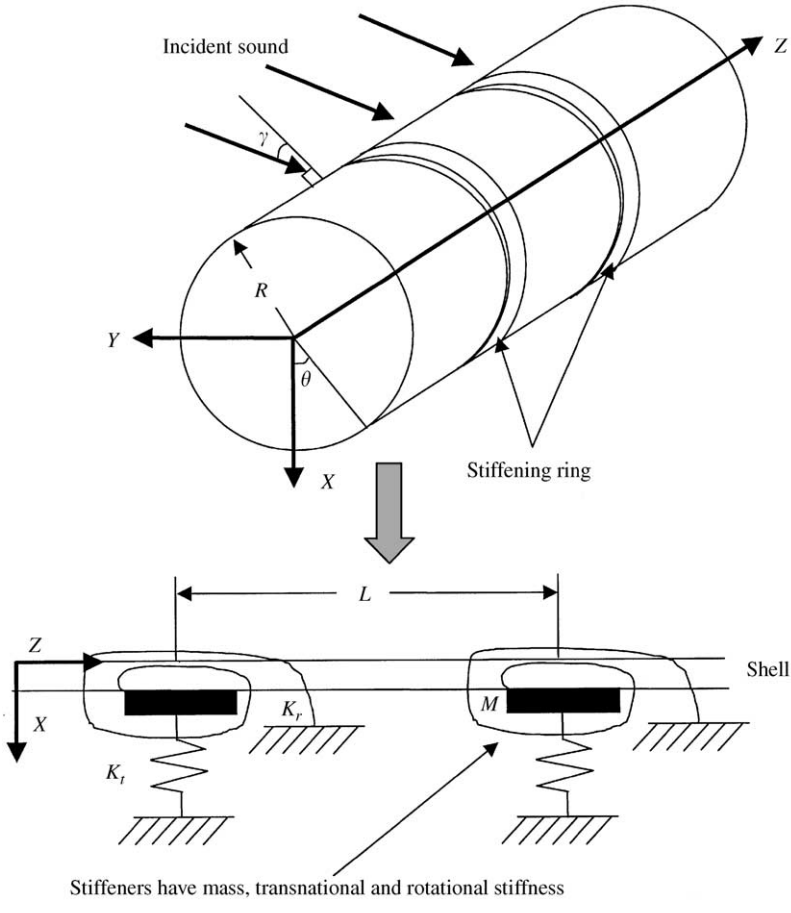

Figure 1. Schematic representation of a stiffened shell.

harmonics as follows:

$$w_1(z,\theta,t) = \sum_{n=0}^{\infty}\sum_{m=-\infty}^{+\infty} w^0_{1nm}\cos[n\theta]\mathrm{e}^{-\mathrm{j}[(\mu+2m\pi)/L]z}\mathrm{e}^{\mathrm{j}\omega t}, \tag{1}$$

$$u_1(z,\theta,t) = \sum_{n=0}^{\infty}\sum_{m=-\infty}^{+\infty} u^0_{1nm}\cos[n\theta]\mathrm{e}^{-\mathrm{j}[(\mu+2m\pi)/L]z}\mathrm{e}^{\mathrm{j}\omega t}, \tag{2}$$

$$v_1(z,\theta,t) = \sum_{n=0}^{\infty}\sum_{m=-\infty}^{+\infty} v^0_{1nm}\sin[n\theta]\mathrm{e}^{-\mathrm{j}[(\mu+2m\pi)/L]z}\mathrm{e}^{\mathrm{j}\omega t}. \tag{3}$$

In equations (1)–(3), $w_1(z,\theta,t)$, $u_1(z,\theta,t)$ and $v_1(z,\theta,t)$ are the displacements of the shell in the transverse, longitudinal directions and circumferential directions, n is the circumferential mode numbers, m is the space harmonic numbers, L is the spacing of stiffeners, and μ is the characteristic propagation constant defined as

$$\frac{\mu}{L} = k_{1z} - \mathrm{j}\psi, \tag{4}$$

where $k_{1z} = k_1 \sin(\gamma)$, $k_1 = \omega/c_1$, and ψ is the phase attenuation coefficient. Expanding the solutions in terms of space harmonics as in equations (1)–(3) is assuming that each subsection of the shell will have the same type of motion with phase delays [2].

The input harmonic plane wave p^I shown in Figure 1 can be described in the cylindrical co-ordinate system as [38]

$$p^I(r, z, \theta, t) = p_0 \sum_{n=0}^{\infty} \varepsilon_n (-j)^n \mathrm{J}_n(k_{1r} r) \cos[n\theta] \, \mathrm{e}^{-\mathrm{j}k_{1z} z} \, \mathrm{e}^{\mathrm{j}\omega t}, \tag{5}$$

where p_0 is the amplitude of the incident wave, $\mathrm{j} = \sqrt{-1}$, $n = 0, 1, 2, 3, \ldots$, J_n is the Bessel function of the first kind of order n, $\varepsilon_0 = 1$ for $n = 0$ and $\varepsilon_n = 2$ for $n = 1, 2, 3, \ldots$, $k_{1r} = k_1 \cos(\gamma)$. It is easily seen that $k_{1r} = \sqrt{k_1^2 - k_{1z}^2}$.

The waves radiated from the shell to the outside p_1^R and into the cavity p_2^T will have the same periodic characteristics as the structural wave in the shell, therefore can be represented as

$$p_1^R(r, z, \theta, t) = \sum_{n=0}^{\infty} \sum_{m=-\infty}^{\infty} p_{1nm}^R H_n^2(k_{1r} r) \cos[n\theta] \mathrm{e}^{-\mathrm{j}[(\mu + 2m\pi)/L]z} \, \mathrm{e}^{\mathrm{j}\omega t}, \tag{6}$$

$$p_2^T(r, z, \theta, t) = \sum_{n=0}^{\infty} \sum_{m=-\infty}^{\infty} p_{2nm}^T H_n^1(k_{2r} r) \cos[n\theta] \mathrm{e}^{-\mathrm{j}[(\mu + 2m\pi)/L]z} \, \mathrm{e}^{\mathrm{j}\omega t}, \tag{7}$$

where $k_{2r} = \sqrt{k_2^2 - k_{2z}^2}$, $k_2 = \omega/c_2$ and H_n^1 and H_n^2 are the Hankel functions of the first and second kind of order n respectively. The former represents the incoming wave and the second the outgoing wave.

2.2. BOUNDARY CONDITIONS AT THE STRUCTURE–ACOUSTIC INTERFACES

The modal amplitudes of the reflected and transmitted acoustic waves can be related to the modal amplitudes of flexural wave in the shell by applying the boundary conditions on the internal and external shell surfaces (i.e., $r = R$). The conditions are from the continuity of the transverse velocities, which are [39]

$$\frac{\partial (p^I + p_1^R)}{\partial r} = -\rho_1 \frac{\partial^2 w_1}{\partial t^2}, \quad \text{at } r = R, \tag{8}$$

$$\frac{\partial p_2^T}{\partial r} = -\rho_2 \frac{\partial^2 w_1}{\partial t^2}, \quad \text{at } r = R. \tag{9}$$

Substituting the assumed solutions into equation (1) and equations (5)–(7) into equation (8) yields the relationship between the modal amplitudes of the reflected wave and the modal amplitudes of flexural wave in the shell as

$$\sum_{n=0}^{\infty} \sum_{m=-\infty}^{\infty} p_{1nm}^R H_n^{2'}(k_{1r} R) k_{1r} \cos[n\theta] \mathrm{e}^{-\mathrm{j}[(\mu + 2m\pi)/L]z}$$
$$= \rho_1 \omega^2 \sum_{n=0}^{\infty} \sum_{m=-\infty}^{\infty} w_{1nm}^0 \cos[n\theta] \mathrm{e}^{-\mathrm{j}[(\mu + 2m\pi)/L]z} - p_0 \sum_{n=0}^{\infty} \varepsilon_n (-j)^n \mathrm{J}_n'(k_{1r} R) k_{1r} \cos[n\theta] \mathrm{e}^{-\mathrm{j}(k_z/L)z}, \tag{10}$$

where $(\,)' = \mathrm{d}/\mathrm{d}r$.

Similarly, substituting the equations into equation (9) yields the relationship between the modal amplitudes of the transmitted wave on the shell, and the modal amplitudes of the

flexural wave in the shell are identified as

$$\sum_{n=0}^{\infty}\sum_{m=-\infty}^{\infty} p_{2nm}^{T} H_n^{1'}(k_{2r}R)k_{2r}\cos[n\theta]\mathrm{e}^{-\mathrm{j}[(\mu+2m\pi)/L]z} = \rho_2\omega^2\sum_{n=0}^{\infty}\sum_{m=-\infty}^{\infty} w_{1nm}^{0}\cos[n\theta]\mathrm{e}^{-\mathrm{j}[(\mu+2m\pi)/L]z}. \tag{11}$$

At each circumferential mode n, the relationship between the modal amplitudes of the reflected waves on the shell and the modal amplitudes of the flexural wave in the shell is identified from equation (10) as

$$p_{1nm}^{R} = \frac{\rho_1\omega^2 w_{1nm}^{0}}{H_n^{2'}(k_{1r}R)k_{1r}} - \frac{p_0\varepsilon_n(-\mathrm{j})^n \mathrm{J}_n'(k_{1r}R)k_{1r}}{H_n^{2'}(k_{1r}R)k_{1r}} \quad \text{for} \quad m=0, \tag{12a}$$

$$= \frac{\rho_1\omega^2 w_{1nm}^{0}}{H_n^{2'}(k_{1r}R)k_{1r}} \quad \text{for} \quad m\neq 0. \tag{12b}$$

Notice that $\mu/L \cong k_z(\omega)$ is assumed to obtain equation (12a) from equation (10) for $m=0$ case, which will be a very close approximation because the phase attenuation coefficient ψ is small and the equation is derived for one span of the structure.

From equation (11), the relationship between the modal amplitudes of the transmitted waves on the shell and the modal amplitudes of flexural wave in the shell is identified as

$$p_{2nm}^{T} = \frac{\rho_2\omega^2 w_{1nm}^{0}}{H_n^{1'}(k_{2r}R)k_{2r}}. \tag{13}$$

2.3. EQUATIONS OF MOTION OF THE SYSTEM

The equations of motion of the system can be derived based on the principle of virtual work following the procedure used by Mead *et al.* [1–3], which states that the virtual displacements applied on the system should not do any work.

Love's equations [37] are used to describe the equations of motion of the cylindrical shell in the axial, circumferential and transverse directions. They are

$$\sum_{n=0}^{\infty}\sum_{m=-\infty}^{\infty} u_{1nm}^{0}\left[K_s\left(\frac{\mu+2m\pi}{L}\right)^2 + \frac{K_s(1-\mu_s)}{2R^2}n^2 - \rho_s h\omega^2\right]\cos[n\theta]\mathrm{e}^{-\mathrm{j}[(\mu+2m\pi)/L]z}$$
$$+\mathrm{j}\frac{K_s(1+\mu_s)}{2R}\sum_{n=0}^{\infty}\sum_{m=-\infty}^{\infty} v_{1nm}^{0} n\left(\frac{\mu+2m\pi}{L}\right)\cos[n\theta]\mathrm{e}^{-\mathrm{j}[(\mu+2m\pi)/L]z}$$
$$+\mathrm{j}\frac{K_s\mu_s}{R}\sum_{n=0}^{\infty}\sum_{m=-\infty}^{\infty} w_{1nm}^{0}\left(\frac{\mu+2m\pi}{L}\right)\cos[n\theta]\mathrm{e}^{-\mathrm{j}[(\mu+2m\pi)/L]z} = 0, \tag{14}$$

$$\sum_{n=0}^{\infty}\sum_{m=-\infty}^{\infty} u_{1nm}^{0}\left[\begin{array}{l}\dfrac{D_s}{R^2}\mu_s\left(\dfrac{\mu+2m\pi}{L}\right)^2 n \\ -\mathrm{j}\left(\dfrac{K_s(1-\mu_s)}{2R}\left(\dfrac{\mu+2m\pi}{L}\right)n + \dfrac{K_s}{R}\mu_s\left(\dfrac{\mu+2m\pi}{L}\right)n\right)\end{array}\right]\sin[n\theta]\mathrm{e}^{-\mathrm{j}[(\mu+2m\pi)/L]z}$$
$$+\sum_{n=0}^{\infty}\sum_{m=-\infty}^{\infty} v_{1nm}^{0}\left[\begin{array}{l}\dfrac{K_s(1-\mu_s)}{2}\left(\dfrac{\mu+2m\pi}{L}\right)^2 + \dfrac{K_s}{R^2}n^2 \\ +\left(\dfrac{D_s(1-\mu_s)}{2R^2}\left(\dfrac{\mu+2m\pi}{L}\right)^2 - \dfrac{D_s}{R^4}n^2 - \rho_s h\omega^2\right)\end{array}\right]\sin[n\theta]\mathrm{e}^{-\mathrm{j}[(\mu+2m\pi)/L]z}$$

$$+\sum_{n=0}^{\infty}\sum_{m=-\infty}^{\infty} w_{1nm}^{0}\left[\frac{K_s}{R^2}n+\frac{D_s(1-\mu_s)}{R^2}\left(\frac{\mu+2m\pi}{L}\right)^2+\frac{D_s}{R^4}n^3\right]\sin[n\theta]\,\mathrm{e}^{-\mathrm{j}[(\mu+2m\pi)/L]z}=0, \quad (15)$$

$$\sum_{n=0}^{\infty}\sum_{m=-\infty}^{\infty} u_{1nm}^{0}\left[D_s\left(\frac{\mu+2m\pi}{L}\right)^4+\frac{D_s}{R^2}\mu_s\left(\frac{\mu+2m\pi}{L}\right)^2 n^2-\mathrm{j}\,\frac{K_s}{R}\mu_s\left(\frac{\mu+2m\pi}{L}\right)\right]\cos[n\theta]\,\mathrm{e}^{-\mathrm{j}[(\mu+2m\pi)/L]z}$$

$$+\sum_{n=0}^{\infty}\sum_{m=-\infty}^{\infty} v_{1nm}^{0}\left[\begin{array}{l}-\dfrac{D_s}{R^2}\mu_s\left(\dfrac{\mu+2m\pi}{L}\right)^2 n\\ +\dfrac{D_s(1-\mu_s)}{R^2}\left(\dfrac{\mu+2m\pi}{L}\right)^2 n-\dfrac{D_s}{R^4}n^3+\dfrac{K_s}{R^2}n\end{array}\right]\cos[n\theta]\,\mathrm{e}^{-\mathrm{j}[(\mu+2m\pi)/L]z}$$

$$+\sum_{n=0}^{\infty}\sum_{m=-\infty}^{\infty} w_{1nm}^{0}\left[\begin{array}{l}\dfrac{D_s\mu_s}{R^2}\left(\dfrac{\mu+2m\pi}{L}\right)^2 n^2+\dfrac{2D_s(1-\mu_s)}{R^2}\left(\dfrac{\mu+2m\pi}{L}\right)^2 n^2\\ +\dfrac{D_s}{R^4}n^4+\dfrac{K_s}{R^2}-\rho_s h\omega^2\end{array}\right]\cos[n\theta]\,\mathrm{e}^{-\mathrm{j}[(\mu+2m\pi)/L]z}$$

$$-p_0\sum_{m=-\infty}^{\infty}\varepsilon_n(-\mathrm{j})^n \mathrm{J}_n(k_{1r}R)\cos[n\theta]\,\mathrm{e}^{-\mathrm{j}(\mu/L)z}-\sum_{n=0}^{\infty}\sum_{m=-\infty}^{\infty} p_{1nm}^{R}H_n^2(k_{1r}R)\cos[n\theta]\,\mathrm{e}^{-\mathrm{j}[(\mu+2m\pi)/L]z}$$

$$+\sum_{n=0}^{\infty}\sum_{m=-\infty}^{\infty} p_{2nm}^{T}H_n^1(k_{2r}R)\cos[n\theta]\,\mathrm{e}^{-\mathrm{j}[(\mu+2m\pi)/L]z}=0, \quad (16)$$

where K_s and D_s are the membrane and bending stiffness of the shell defined as [37]

$$K_s=\frac{E_s(1-\mathrm{j}\eta_s)h}{1-\mu_s^2}, \qquad D_s=\frac{E_s(1-\mathrm{j}\eta_s)h^3}{12(1-\mu_s^2)}, \quad (17, 18)$$

where η_s is the shell loss factor [40]. Because the inertia terms are represented in the D'Alembert equivalent forces in equations (14)–(16), the equations represent the equivalent forces acting on a shell of unit axial and circumferential length in three directions.

From the assumed displacements in equations (1)–(3), the virtual displacement can be expressed as any one of the sets of three displacements in the transverse, circumferential and longitudinal directions, described as

$$\delta w_{pq}=\delta w\cos[q\theta]\,\mathrm{e}^{-\mathrm{j}[(\mu+2p\pi)/L]z}\,\mathrm{e}^{\mathrm{j}\omega t}, \quad (19a)$$

$$\delta v_{pq}=\delta v\sin[q\theta]\,\mathrm{e}^{-\mathrm{j}[(\mu+2p\pi)/L]z}\,\mathrm{e}^{\mathrm{j}\omega t}, \quad (19b)$$

$$\delta u_{pq}=\delta u\cos[q\theta]\,\mathrm{e}^{-\mathrm{j}[(\mu+2p\pi)/L]z}\,\mathrm{e}^{\mathrm{j}\omega t}. \quad (19c)$$

Because complex algebra is used, the conjugate forms of the virtual displacements are multiplied with the equivalent forces to calculate the virtual work.

The virtual work done by the cylindrical shell alone (without stiffeners) is obtained first. The work done by each virtual displacement is obtained by integrating the product of

the virtual displacement (conjugate form) and the equivalent force in the corresponding direction. The work done by the longitudinal virtual displacement is obtained as

$$\delta\Pi_{su} = \delta u^* \left\{ \int_0^{2\pi} R \int_0^L \sum_{n=0}^{\infty} \sum_{m=-\infty}^{\infty} u^0_{1nm} \left[\begin{array}{l} K_s \left(\dfrac{\mu + 2m\pi}{L} \right)^2 \\ + \dfrac{K_s(1-\mu_s)}{2R^2} n^2 \\ - \rho_s h \omega^2 \end{array} \right] \mathrm{e}^{-\mathrm{j}[(\mu+2m\pi)/L]z} \mathrm{e}^{\mathrm{j}[(\mu+2p\pi)/L]z} \right.$$

$$\times \cos[n\theta] \cos[q\theta] \, \mathrm{d}z \, \mathrm{d}\theta$$

$$+ \mathrm{j} \frac{K_s(1+\mu_s)}{2R} \int_0^{2\pi} R \int_0^L \sum_{n=0}^{\infty} \sum_{m=-\infty}^{\infty} v^0_{1nm} n \left(\frac{\mu + 2m\pi}{L} \right) \mathrm{e}^{-\mathrm{j}[(\mu+2m\pi)/L]z} \mathrm{e}^{\mathrm{j}[(\mu+2p\pi)/L]z} \cos[n\theta]$$

$$\times \cos[q\theta] \, \mathrm{d}z \, \mathrm{d}\theta$$

$$+ \mathrm{j} \frac{K_s \mu_s}{R} \int_0^{2\pi} R \int_0^L \sum_{n=0}^{\infty} \sum_{m=-\infty}^{\infty} w^0_{1nm} \left(\frac{\mu + 2m\pi}{L} \right) \mathrm{e}^{-\mathrm{j}[(\mu+2m\pi)/L]z} \mathrm{e}^{\mathrm{j}[(\mu+2p\pi)/L]z} \cos[n\theta]$$

$$\left. \times \cos[q\theta] \, \mathrm{d}z \, \mathrm{d}\theta \right\}. \tag{20}$$

The work done by the circumferential virtual displacement becomes

$$\delta\Pi_{sv} = \delta v^* \left\{ \int_0^{2\pi} R \int_0^L \sum_{n=0}^{\infty} \sum_{m=-\infty}^{\infty} u^0_{1nm} \left[\begin{array}{l} \dfrac{D_s}{R^2} \mu_s \left(\dfrac{\mu + 2m\pi}{L} \right)^2 n \\ - \mathrm{j} \left(\dfrac{K_s(1-\mu_s)}{2R} \left(\dfrac{\mu + 2m\pi}{L} \right) n \right) \\ \quad + \dfrac{K_s}{R} \mu_s \left(\dfrac{\mu + 2m\pi}{L} \right) n \end{array} \right] \right.$$

$$\times \mathrm{e}^{-\mathrm{j}[(\mu+2m\pi)/L]z} \mathrm{e}^{-\mathrm{j}[(\mu+2p\pi)/L]z} \sin[n\theta] \sin[q\theta] \, \mathrm{d}z \, \mathrm{d}\theta$$

$$+ \int_0^{2\pi} R \int_0^L \sum_{n=0}^{\infty} \sum_{m=-\infty}^{\infty} v^0_{1nm} \left[\begin{array}{l} \dfrac{K_s(1-\mu_s)}{2} \left(\dfrac{\mu + 2m\pi}{L} \right)^2 + \dfrac{K_s}{R^2} n^2 \\ + \dfrac{D_s(1-\mu_s)}{2R^2} \left(\dfrac{\mu + 2m\pi}{L} \right)^2 \\ - \dfrac{D_s}{R^4} n^2 - \rho_s h \omega^2 \end{array} \right] \mathrm{e}^{-\mathrm{j}[(\mu+2m\pi)/L]z} \mathrm{e}^{-\mathrm{j}[(\mu+2p\pi)/L]z}$$

$$\times \sin[n\theta]\sin[q\theta]\,\mathrm{d}z\,\mathrm{d}\theta + \int_0^{2\pi} R \int_0^L \sum_{n=0}^{\infty}\sum_{m=-\infty}^{\infty} w_{1nm}^0 \left[\begin{array}{l} \dfrac{K_s}{R^2}n + \dfrac{D_s(1-\mu_s)}{R^2}\left(\dfrac{\mu+2m\pi}{L}\right)^2 \\ \quad + \dfrac{D_s}{R^4}n^3 \end{array}\right]$$

$$\times \mathrm{e}^{-\mathrm{j}[(\mu+2m\pi)/L]z}\,\mathrm{e}^{-\mathrm{j}[(\mu+2p\pi)/L]z}\sin[n\theta]\sin[q\theta]\,\mathrm{d}z\,\mathrm{d}\theta \Bigg\}. \tag{21}$$

The work done by the transverse virtual displacement becomes

$$\delta\Pi_{su} = \delta w^* \Bigg\{ \int_0^{2\pi} R \int_0^L \sum_{n=0}^{\infty}\sum_{m=-\infty}^{\infty} u_{1nm}^0 \left[\begin{array}{l} D_s\left(\dfrac{\mu+2m\pi}{L}\right)^4 \\ \quad + \dfrac{D_s}{R^2}\mu_s\left(\dfrac{\mu+2m\pi}{L}\right)^2 n^2 \\ \quad - \mathrm{j}\dfrac{K_s}{R}\mu_s\left(\dfrac{\mu+2m\pi}{L}\right) \end{array}\right]$$

$$\times \mathrm{e}^{-\mathrm{j}[(\mu+2m\pi)/L]z}\,\mathrm{e}^{-\mathrm{j}[(\mu+2p\pi)/L]z}\cos[n\theta]\cos[q\theta]\,\mathrm{d}z\,\mathrm{d}\theta$$

$$+ \int_0^{2\pi} R \int_0^L \sum_{n=0}^{\infty}\sum_{m=-\infty}^{\infty} v_{1nm}^0 \left[\begin{array}{l} -\dfrac{D_s}{R^2}\mu_s\left(\dfrac{\mu+2m\pi}{L}\right)^2 n \\ \quad + \dfrac{D_s(1-\mu_s)}{R^2}\left(\dfrac{\mu+2m\pi}{L}\right)^2 n - \dfrac{D_s}{R^4}n^3 + \dfrac{K_s}{R^2}n \end{array}\right]$$

$$\times \mathrm{e}^{-\mathrm{j}[(\mu+2m\pi)/L]z}\,\mathrm{e}^{-\mathrm{j}[(\mu+2p\pi)/L]z}\cos[n\theta]\cos[q\theta]\,\mathrm{d}z\,\mathrm{d}\theta$$

$$+ \int_0^{2\pi} R \int_0^L \sum_{n=0}^{\infty}\sum_{m=-\infty}^{\infty} w_{1nm}^0 \left[\begin{array}{l} \dfrac{D_s\mu_s}{R^2}\left(\dfrac{\mu+2m\pi}{L}\right)^2 n^2 \\ \quad + \dfrac{2D_s(1-\mu_s)}{R^2}\left(\dfrac{\mu+2m\pi}{L}\right)^2 n^2 \\ \quad + \dfrac{D_s}{R^4}n^4 + \dfrac{K_s}{R^2} - \rho_s h\omega^2 \end{array}\right] \mathrm{e}^{-\mathrm{j}[(\mu+2m\pi)/L]z}\,\mathrm{e}^{\mathrm{j}[(\mu+2p\pi)/L]z}$$

$$\times \cos[n\theta]\cos[q\theta]\,\mathrm{d}z\,\mathrm{d}\theta$$

$$- \int_0^{2\pi} R \int_0^L \left[\begin{array}{l} p_0 \sum_{m=-\infty}^{\infty} \varepsilon_n(-\mathrm{j})^n \mathrm{J}_n(k_{1r}R)\mathrm{e}^{-\mathrm{j}(\mu/\mathrm{L})z} \\ \quad + \sum_{n=0}^{\infty}\sum_{m=-\infty}^{\infty} p_{1nm}^R H_n^2(k_{1r}R)\mathrm{e}^{-\mathrm{j}[(\mu+2m\pi)/L]z} \\ \quad - \sum_{n=0}^{\infty}\sum_{m=-\infty}^{\infty} p_{1nm}^T H_n^2(k_{1r}R)\mathrm{e}^{-\mathrm{j}[(\mu+2m\pi)/L]z} \end{array}\right] \mathrm{e}^{\mathrm{j}[(\mu+2p\pi)/L]z}\cos[n\theta]\cos[q\theta]\,\mathrm{d}z\,\mathrm{d}\theta \Bigg\}. \tag{22}$$

The virtual work done by the translational spring is obtained as

$$\delta\Pi_t = K_t w_1(0,\theta,t)\,\delta w^*_{pq} = \delta w^* K_t \int_0^{2\pi} R \sum_{n=0}^{\infty}\sum_{m=-\infty}^{\infty} w^0_{1nm}\cos[n\theta]\cos[q\theta]\,\mathrm{d}\theta. \tag{23}$$

All three virtual displacements contribute to the work done by the rotational spring, therefore,

$$\begin{aligned}\delta\Pi_r &= \mathrm{j}K_r\left(\frac{\mu+2p\pi}{L}\right)(u_1'(0,\theta,t)\delta u^*_{pq} + v_1'(0,\theta,t)\delta v^*_{pq} + w_1'(0,\theta,t)\delta w^*_{pq})\\
&= \delta u^* K_r\left(\frac{\mu+2p\pi}{L}\right)\int_0^{2\pi} R\sum_{n=0}^{\infty}\sum_{m=-\infty}^{\infty} u^0_{1nm}\left(\frac{\mu+2m\pi}{L}\right)\cos[n\theta]\cos[q\theta]\,\mathrm{d}\theta\\
&\quad + \delta v^* K_r\left(\frac{\mu+2p\pi}{L}\right)\int_0^{2\pi} R\sum_{n=0}^{\infty}\sum_{m=-\infty}^{\infty} v^0_{1nm}\left(\frac{\mu+2m\pi}{L}\right)\sin[n\theta]\sin[q\theta]\,\mathrm{d}\theta\\
&\quad + \delta w^* K_r\left(\frac{\mu+2p\pi}{L}\right)\int_0^{2\pi} R\sum_{n=0}^{\infty}\sum_{m=-\infty}^{\infty} w^0_{1nm}\left(\frac{\mu+2m\pi}{L}\right)\cos[n\theta]\cos[q\theta]\,\mathrm{d}\theta.\end{aligned} \tag{24}$$

The virtual work done by the lumped mass becomes

$$\delta\Pi_M = -\omega^2 M w_1(0,\theta,t)\delta w^*_{pq} = -\omega^2 M\delta w^* \int_0^{2\pi} R\sum_{n=0}^{\infty}\sum_{m=-\infty}^{\infty} w^0_{1nm}\cos[n\theta]\cos[q\theta]\,\mathrm{d}\theta. \tag{25}$$

Notice that the co-ordinate of $z = 0$ and $r = R$ is taken to calculate the work done by the springs and mass because only one set has to be considered.

The virtual work principle requires that

$$\delta\Pi_{su} + \delta\Pi_{sv} + \delta\Pi_{sw} + \delta\Pi_t + \delta\Pi_r + \delta\Pi_M = 0. \tag{26}$$

Because of the orthogonal property of the trigonometric functions, integrating equations (20)–(26) with respect to z and θ yields the following.

When $p \neq 0$:

$$\left\{\begin{array}{l} u^0_{1np}\left[\begin{array}{l} K_s\left(\dfrac{\mu+2p\pi}{L}\right)^2 + \dfrac{K_s(1-\mu_s)}{2R^2}n^2 \\ -\rho_s h\omega^2 \end{array}\right] + v^0_{1np}\dfrac{K_s(1+\mu_s)}{2R}n\left(\dfrac{\mu+2p\pi}{L}\right)\mathrm{j} \\ + w^0_{1np}\dfrac{K_s\mu_s}{R}\left(\dfrac{\mu+2p\pi}{L}\right)\mathrm{j} + \dfrac{K_r}{L}\displaystyle\sum_{m=-\infty}^{\infty} u^0_{1nm}\left(\dfrac{\mu+2m\pi}{L}\right)\left(\dfrac{\mu+2p\pi}{L}\right) \end{array}\right\}\delta u^*$$

$$
+\left\{\begin{array}{l}
u_{1np}^{0}\left[\begin{array}{l}\dfrac{D_s}{R^2}\mu_s\left(\dfrac{\mu+2p\pi}{L}\right)^2 n-\mathrm{j}\left(\begin{array}{l}\dfrac{K_s(1-\mu_s)}{2R}\left(\dfrac{\mu+2p\pi}{L}\right)n\\ +\dfrac{K_s}{R}\mu_s\left(\dfrac{\mu+2p\pi}{L}\right)n\end{array}\right)\end{array}\right]\\
+v_{1np}^{0}\left[\begin{array}{l}\dfrac{K_s(1-\mu_s)}{2}\left(\dfrac{\mu+2p\pi}{L}\right)^2+\dfrac{K_s}{R^2}n^2+\dfrac{D_s(1-\mu_s)}{2R^2}\left(\dfrac{\mu+2p\pi}{L}\right)^2\\ -\dfrac{D_s}{R^4}n^2-\rho_s h\omega^2\end{array}\right]\\
+w_{1np}^{0}\left[\dfrac{K_s}{R^2}n+\dfrac{D_s(1-\mu_s)}{R^2}\left(\dfrac{\mu+2p\pi}{L}\right)^2+\dfrac{D_s}{R^4}n^3\right]\\
+\dfrac{K_r}{L}\displaystyle\sum_{m=-\infty}^{\infty}v_{1nm}^{0}\left(\dfrac{\mu+2m\pi}{L}\right)\left(\dfrac{\mu+2p\pi}{L}\right)
\end{array}\right\}\delta v^{*}
$$

$$
+\left\{\begin{array}{l}
u_{1np}^{0}\left[\begin{array}{l}D_s\left(\dfrac{\mu+2p\pi}{L}\right)^4+\dfrac{D_s}{R^2}\mu_s\left(\dfrac{\mu+2p\pi}{L}\right)^2 n^2\\ -\mathrm{j}\dfrac{K_s}{R}\mu_s\left(\dfrac{\mu+2p\pi}{L}\right)\end{array}\right]\\
+v_{1np}^{0}\left[-\dfrac{D_s}{R^2}\mu_s\left(\dfrac{\mu+2p\pi}{L}\right)^2 n+\dfrac{D_s(1-\mu_s)}{R^2}\left(\dfrac{\mu+2p\pi}{L}\right)^2 n-\dfrac{D_s}{R^4}n^3+\dfrac{K_s}{R^2}n\right]\\
+w_{1np}^{0}\left[\begin{array}{l}\dfrac{D_s\mu_s}{R^2}\left(\dfrac{\mu+2p\pi}{L}\right)^2 n^2+\dfrac{2D_s(1-\mu_s)}{R^2}\left(\dfrac{\mu+2p\pi}{L}\right)^2 n^2\\ +\dfrac{D_s}{R^4}n^4+\dfrac{K_s}{R^2}-\rho_s h\omega^2\\ -\dfrac{H_n^2(k_{1r}R)\rho_1\omega^2}{H_n^{2'}(k_{1r}R)k_{1r}}+\dfrac{H_n^1(k_{2r}R)\rho_2\omega^2}{H_n^{1'}(k_{2r}R)k_{2r}}\end{array}\right]\\
+\left(\dfrac{K_t}{L}-\dfrac{\omega^2 M}{L}\right)\displaystyle\sum_{m=-\infty}^{\infty}w_{1nm}^{0}+\dfrac{K_r}{L}\sum_{m=-\infty}^{\infty}w_{1nm}^{0}\left(\dfrac{\mu+2m\pi}{L}\right)\left(\dfrac{\mu+2p\pi}{L}\right)\\
-p_0\left[\varepsilon_n(-\mathrm{j})^n\mathrm{J}_n(k_{1r}R)-\dfrac{\varepsilon_n(-\mathrm{j})^n H_n^2(k_{2r}R)\mathrm{J}_n'(k_{1r}R)k_{1r}}{H_n^{2'}(k_{1r}R)k_{1r}}\right]
\end{array}\right\}\delta w^{*} \quad (27)
$$

$$
=0.
$$

When $p \neq 0$:

$$
\left\{ \begin{array}{l} u^0_{1np}\left[\begin{array}{l} K_s\left(\dfrac{\mu+2p\pi}{L}\right)^2 + \dfrac{K_s(1-\mu_s)}{2R^2}n^2 \\ -\rho_s h\omega^2 \end{array} \right] + v^0_{1np}\dfrac{K_s(1+\mu_s)}{2R}n\left(\dfrac{\mu+2p\pi}{L}\right)\mathrm{j} \\ + w^0_{1np}\dfrac{K_s\mu_s}{R}\left(\dfrac{\mu+2p\pi}{L}\right)\mathrm{j} + \dfrac{K_r}{L}\sum\limits_{m=-\infty}^{\infty} u^0_{1nm}\left(\dfrac{\mu+2m\pi}{L}\right)\left(\dfrac{\mu+2p\pi}{L}\right) \end{array} \right\} \delta u^*
$$

$$
+ \left\{ \begin{array}{l} u^0_{1np}\left[\dfrac{D_s}{R^2}\mu_s\left(\dfrac{\mu+2p\pi}{L}\right)^2 n - \mathrm{j}\left(\begin{array}{l} \dfrac{K_s(1-\mu_s)}{2R}\left(\dfrac{\mu+2p\pi}{L}\right)n \\ + \dfrac{K_s}{R}\mu_s\left(\dfrac{\mu+2p\pi}{L}\right)n \end{array} \right) \right] \\ + v^0_{1np}\left[\begin{array}{l} \dfrac{K_s(1-\mu_s)}{2}\left(\dfrac{\mu+2p\pi}{L}\right)^2 + \dfrac{K_s}{R^2}n^2 + \dfrac{D_s(1-\mu_s)}{2R^2}\left(\dfrac{\mu+2p\pi}{L}\right)^2 \\ -\dfrac{D_s}{R^4}n^2 - \rho_s h\omega^2 \end{array} \right] \\ + w^0_{1np}\left[\dfrac{K_s}{R^2}n + \dfrac{D_s(1-\mu_s)}{R^2}\left(\dfrac{\mu+2p\pi}{L}\right)^2 + \dfrac{D_s}{R^4}n^3\right] \\ + \dfrac{K_r}{L}\sum\limits_{m=-\infty}^{\infty} v^0_{1nm}\left(\dfrac{\mu+2m\pi}{L}\right)\left(\dfrac{\mu+2p\pi}{L}\right) \end{array} \right\} \delta v^*
$$

$$
+ \left\{ \begin{array}{l} u^0_{1np}\left[\begin{array}{l} D_s\left(\dfrac{\mu+2p\pi}{L}\right)^4 + \dfrac{D_s}{R^2}\mu_s\left(\dfrac{\mu+2p\pi}{L}\right)^2 n^2 \\ -\mathrm{j}\dfrac{K_s}{R}\mu_s\left(\dfrac{\mu+2p\pi}{L}\right) \end{array} \right] \\ + v^0_{1np}\left[-\dfrac{D_s}{R^2}\mu_s\left(\dfrac{\mu+2p\pi}{L}\right)^2 n + \dfrac{D_s(1-\mu_s)}{R^2}\left(\dfrac{\mu+2p\pi}{L}\right)^2 n - \dfrac{D_s}{R^4}n^3 + \dfrac{K_s}{R^2}n \right] \\ + w^0_{1np}\left[\begin{array}{l} \dfrac{D_s\mu_s}{R^2}\left(\dfrac{\mu+2p\pi}{L}\right)^2 n^2 + \dfrac{2D_s(1-\mu_s)}{R^2}\left(\dfrac{\mu+2p\pi}{L}\right)^2 n^2 \\ + \dfrac{D_s}{R^4}n^4 + \dfrac{K_s}{R^2} - \rho_s h\omega^2 \\ -\dfrac{H^2_n(k_{1r}R)\rho_1\omega^2}{H^{2'}_n(k_{1r}R)k_{1r}} + \dfrac{H^1_n(k_{2r}R)\rho_2\omega^2}{H^{1'}_n(k_{2r}R)k_{2r}} \end{array} \right] \\ + \left(\dfrac{K_t}{L} - \dfrac{\omega^2 M}{L}\right)\sum\limits_{m=-\infty}^{\infty} w^0_{1nm} + \dfrac{K_r}{L}\sum\limits_{m=-\infty}^{\infty} w^0_{1nm}\left(\dfrac{\mu+2m\pi}{L}\right)\left(\dfrac{\mu+2p\pi}{L}\right) \end{array} \right\} \delta w^*
$$

$$
= 0. \tag{28}
$$

Because δu^*, δv^* and δw^* in equations (27)–(28) are virtual displacements, which are arbitrary, each coefficient of the three virtual displacements should become zero for the equations to be satisfied. Thus, we obtain three equations of motion for each $n = 0, 1, 2, 3, \ldots$, and for m, p, where $p = 0, \pm 1, \pm 2, \pm 3, \pm 4, \ldots$:

$$u^0_{1np}\left[\begin{array}{l} K_s\left(\dfrac{\mu+2p\pi}{L}\right)^2 + \dfrac{K_s(1-\mu_s)}{2R^2}n^2 \\ \\ -\rho_s h\omega^2 \end{array}\right] + v^0_{1np}\frac{K_s(1+\mu_s)}{2R}n\left(\frac{\mu+2p\pi}{L}\right)\mathrm{j}$$

$$+ w^0_{1np}\frac{K_s\mu_s}{R}\left(\frac{\mu+2p\pi}{L}\right)\mathrm{j} + \frac{K_r}{L}\sum_{m=-\infty}^{\infty} u^0_{1nm}\left(\frac{\mu+2m\pi}{L}\right)\left(\frac{\mu+2p\pi}{L}\right) = 0, \tag{29}$$

$$u^0_{1np}\left[\frac{D_s}{R^2}\mu_s\left(\frac{\mu+2p\pi}{L}\right)^2 n - \mathrm{j}\left(\frac{K_s(1-\mu_s)}{2R}\left(\frac{\mu+2p\pi}{L}\right)n + \frac{K_s}{R}\mu_s\left(\frac{\mu+2p\pi}{L}\right)n\right)\right]$$

$$+ v^0_{1np}\left[\frac{K_s(1-\mu_s)}{2}\left(\frac{\mu+2p\pi}{L}\right)^2 + \frac{K_s}{R^2}n^2 + \frac{D_s(1-\mu_s)}{2R^2}\left(\frac{\mu+2p\pi}{L}\right)^2 - \frac{D_s}{R^4}n^2 - \rho_s h\omega^2\right]$$

$$+ w^0_{1np}\left[\frac{K_s}{R^2}n + \frac{D_s(1-\mu_s)}{R^2}\left(\frac{\mu+2p\pi}{L}\right)^2 + \frac{D_s}{R^4}n^3\right] + \frac{K_r}{L}\sum_{m=-\infty}^{\infty} v^0_{1nm}\left(\frac{\mu+2m\pi}{L}\right)\left(\frac{\mu+2p\pi}{L}\right) = 0, \tag{30}$$

$$u^0_{1np}\left[\begin{array}{l} D_s\left(\dfrac{\mu+2p\pi}{L}\right)^4 + \dfrac{D_s}{R^2}\mu_s\left(\dfrac{\mu+2p\pi}{L}\right)^2 n^2 \\ \\ -\mathrm{j}\dfrac{K_s}{R}\mu_s\left(\dfrac{\mu+2p\pi}{L}\right) \end{array}\right]$$

$$+ v^0_{1np}\left[-\frac{D_s}{R^2}\mu_s\left(\frac{\mu+2p\pi}{L}\right)^2 n + \frac{D_s(1-\mu_s)}{R^2}\left(\frac{\mu+2p\pi}{L}\right)^2 n - \frac{D_s}{R^4}n^3 + \frac{K_s}{R^2}n\right]$$

$$+ w^0_{1np}\left[\begin{array}{l} \dfrac{D_s\mu_s}{R^2}\left(\dfrac{\mu+2p\pi}{L}\right)^2 n^2 + \dfrac{2D_s(1-\mu_s)}{R^2}\left(\dfrac{\mu+2p\pi}{L}\right)^2 n^2 \\ \\ \quad + \dfrac{D_s}{R^4}n^4 + \dfrac{K_s}{R^2} - \rho_s h\omega^2 \\ \\ \quad - \dfrac{H^2_n(k_{1r}R)\rho_1\omega^2}{H^{2'}_n(k_{1r}R)k_{1r}} + \dfrac{H^1_n(k_{2r}R)\rho_2\omega^2}{H^{1'}_n(k_{2r}R)k_{2r}} \end{array}\right]$$

$$+ \left(\frac{K_t}{L} - \frac{\omega^2 M}{L}\right)\sum_{m=-\infty}^{\infty} w^0_{1nm} + \frac{K_r}{L}\sum_{m=-\infty}^{\infty} w^0_{1nm}\left(\frac{\mu+2m\pi}{L}\right)\left(\frac{\mu+2p\pi}{L}\right)$$

$$= p_0\left[\varepsilon_n(-\mathrm{j})^n \mathrm{J}_n(k_{1r}R) - \frac{\varepsilon_n(-\mathrm{j})^n H^2_n(k_{2r}R)\mathrm{J}'_n(k_{1r}R)k_{1r}}{H^{2'}_n(k_{1r}R)k_{1r}}\right], \qquad \text{when } p = 0, \tag{31a}$$

$$= 0, \qquad \text{when } p \neq 0. \tag{31b}$$

This constitutes a set of simultaneous equations for u^0_{1np}, v^0_{1np} and w^0_{1np}. Consideration of the virtual work in any other shell element would yield an identical set of equations. Finite terms

have to be taken to solve equations (29)–(31). In the actual calculation in this work, $p = -5$ to 5, 11 space harmonic terms were used after the convergence consideration. Also notice that the series of m in equations (29)–(31) was also summed from $m = -5$ to 5 in this case. For the purpose of easier explanation, the 3 term space harmonic solution case is explained. In this case $p = -1, 0$, and 1, and the space mode is summed for $m = -1$, 0, 1. This yields nine simultaneous equations for $w^0_{1n-1}, w^0_{1n0}, w^0_{1n1}, u^0_{1n-1}, u^0_{1n0}, u^0_{1n1}, v^0_{1n-1}, v^0_{1n0}$ and v^0_{1n1} at each n. Then, equation (31) can be put into a matrix equation:

$$\begin{bmatrix} A1 & B1 & C1 & D1 & 0 & 0 & E1 & 0 & 0 \\ F1 & G1 & H1 & 0 & I1 & 0 & 0 & J1 & 0 \\ K1 & L1 & M1 & 0 & 0 & N1 & 0 & 0 & O1 \\ P1 & 0 & 0 & Q1 & R1 & S1 & T1 & 0 & 0 \\ 0 & U1 & 0 & V1 & W1 & X1 & 0 & Y1 & 0 \\ 0 & 0 & Z1 & A2 & B2 & C2 & 0 & 0 & D2 \\ E2 & 0 & 0 & F2 & 0 & 0 & G2 & H2 & I2 \\ 0 & J2 & 0 & 0 & K2 & 0 & L2 & M2 & N2 \\ 0 & 0 & P2 & 0 & 0 & Q2 & R2 & S2 & T2 \end{bmatrix} \begin{Bmatrix} u_{1n-1} \\ u_{1n0} \\ u_{1n1} \\ v_{1n-1} \\ v_{1n0} \\ v_{1n1} \\ w_{1n-1} \\ w_{1n0} \\ w_{1n1} \end{Bmatrix} = \begin{Bmatrix} 0 \\ 0 \\ 0 \\ 0 \\ 0 \\ 0 \\ 0 \\ O2 \\ 0 \end{Bmatrix}, \tag{32}$$

where

$$A1 = K_s\left(\frac{\mu + 2(-1)\pi}{L}\right)^2 + \frac{K_s(1-\mu_s)}{2R^2}n^2 - \rho_s h\omega^2 + \frac{K_r}{L}\left(\frac{\mu + 2(-1)\pi}{L}\right)^2,$$

$$B1 = \frac{K_r}{L}\left(\frac{\mu + 2(0)\pi}{L}\right)\left(\frac{\mu + 2(-1)\pi}{L}\right), \quad C1 = \frac{K_r}{L}\left(\frac{\mu + 2(1)\pi}{L}\right)\left(\frac{\mu + 2(-1)\pi}{L}\right),$$

$$D1 = \frac{K_s(1+\mu_s)}{2R}n\left(\frac{\mu + 2(-1)\pi}{L}\right)j, \quad E1 = \frac{K_s\mu_s}{L}\left(\frac{\mu + 2(-1)\pi}{L}\right)j,$$

$$F1 = \frac{K_r}{L}\left(\frac{\mu + 2(-1)\pi}{L}\right)\left(\frac{\mu + 2(0)\pi}{L}\right),$$

$$G1 = K_s\left(\frac{\mu + 2(0)\pi}{L}\right)^2 + \frac{K_s(1-\mu_s)}{2R^2}n^2 - \rho_s h\omega^2 + \frac{K_r}{L}\left(\frac{\mu + 2(0)\pi}{L}\right)^2,$$

$$H1 = \frac{K_r}{L}\left(\frac{\mu + 2(1)\pi}{L}\right)\left(\frac{\mu + 2(0)\pi}{L}\right), \quad I1 = \frac{K_s(1+\mu_s)}{2R}n\left(\frac{\mu + 2(0)\pi}{L}\right)j,$$

$$J1 = \frac{K_s\mu_s}{R}\left(\frac{\mu + 2(0)\pi}{L}\right)j, \quad K1 = \frac{K_r}{L}\left(\frac{\mu + 2(-1)\pi}{L}\right)\left(\frac{\mu + 2(1)\pi}{L}\right),$$

$$L1 = \frac{K_r}{L}\left(\frac{\mu + 2(0)\pi}{L}\right)\left(\frac{\mu + 2(1)\pi}{L}\right),$$

$$M1 = K_s\left(\frac{\mu + 2(1)\pi}{L}\right)^2 + \frac{K_s(1-\mu_s)}{2R^2}n^2 - \rho_s h\omega^2 + \frac{K_r}{L}\left(\frac{\mu + 2(1)\pi}{L}\right)^2,$$

$$N1 = \frac{K_s(1+\mu_s)}{2R}n\left(\frac{\mu + 2(1)\pi}{L}\right)j, \quad O1 = \frac{K_s\mu_s}{R}\left(\frac{\mu + 2(1)\pi}{L}\right)j,$$

$$P1 = \frac{D_s}{R^2}\mu_s\left(\frac{\mu + 2(-1)\pi}{L}\right)^2 n - j\left(\frac{K_s(1-\mu_s)}{2R}\left(\frac{\mu + 2(-1)\pi}{L}\right)n + \frac{K_s}{R}\mu_s\left(\frac{\mu + 2(-1)\pi}{L}\right)n\right),$$

$$Q1 = \frac{K_s(1-\mu_s)}{2}\left(\frac{\mu + 2(-1)\pi}{L}\right)^2 + \frac{K_s}{R^2}n^2 + \frac{D_s(1-\mu_s)}{2R^2}\left(\frac{\mu + 2(-1)\pi}{L}\right)^2$$
$$- \frac{D_s}{R^4}n^2 - \rho_s h\omega^2 + \frac{K_r}{L}\left(\frac{\mu + 2(-1)\pi}{L}\right)^2,$$

$$R1 = \frac{K_r}{L}\left(\frac{\mu + 2(0)\pi}{L}\right)\left(\frac{\mu + 2(-1)\pi}{L}\right), \quad S1 = \frac{K_r}{L}\left(\frac{\mu + 2(1)\pi}{L}\right)\left(\frac{\mu + 2(-1)\pi}{L}\right),$$

$$T1 = \frac{K_s}{R^2}n + \frac{D_s(1-\mu_s)}{R^2}\left(\frac{\mu + 2(-1)\pi}{L}\right)^2 + \frac{D_s}{R^4}n^3,$$

$$U1 = \frac{D_s}{R^2}\mu_s\left(\frac{\mu + 2(0)\pi}{L}\right)^2 n - \mathrm{j}\left(\frac{K_s(1-\mu_s)}{2R}\left(\frac{\mu + 2(0)\pi}{L}\right)n + \frac{K_s}{R}\mu_s\left(\frac{\mu + 2(0)\pi}{L}\right)n\right),$$

$$V1 = \frac{K_r}{L}\left(\frac{\mu + 2(-1)\pi}{L}\right)\left(\frac{\mu + 2(0)\pi}{L}\right),$$

$$W1 = \frac{K_s(1-\mu_s)}{2}\left(\frac{\mu + 2(0)\pi}{L}\right)^2 + \frac{K_s}{R^2}n^2 + \frac{D_s(1-\mu_s)}{2R^2}\left(\frac{\mu + 2(0)\pi}{L}\right)^2$$
$$- \frac{D_s}{R^4}n^2 - \rho_s h\omega^2 + \frac{K_r}{L}\left(\frac{\mu + 2(0)\pi}{L}\right)^2,$$

$$X1 = \frac{K_r}{L}\left(\frac{\mu + 2(1)\pi}{L}\right)\left(\frac{\mu + 2(0)\pi}{L}\right), \quad Y1 = \frac{K_s}{R^2}n + \frac{D_s(1-\mu_s)}{R^2}\left(\frac{\mu + 2(0)\pi}{L}\right)^2 + \frac{D_s}{R^4}n^3,$$

$$Z1 = \frac{D_s}{R^2}\mu_s\left(\frac{\mu + 2(1)\pi}{L}\right)^2 n - \mathrm{j}\left(\frac{K_s(1-\mu_s)}{2R}\left(\frac{\mu + 2(1)\pi}{L}\right)n + \frac{K_s}{R}\mu_s\left(\frac{\mu + 2(1)\pi}{L}\right)n\right),$$

$$A2 = \frac{K_r}{L}\left(\frac{\mu + 2(-1)\pi}{L}\right)\left(\frac{\mu + 2(1)\pi}{L}\right), \quad B2 = \frac{K_r}{L}\left(\frac{\mu + 2(0)\pi}{L}\right)\left(\frac{\mu + 2(1)\pi}{L}\right),$$

$$C2 = \frac{K_s(1-\mu_s)}{2}\left(\frac{\mu + 2(1)\pi}{L}\right)^2 + \frac{K_s}{R^2}n^2 + \frac{D_s(1-\mu_s)}{2R^2}\left(\frac{\mu + 2(1)\pi}{L}\right)^2$$
$$- \frac{D_s}{R^4}n^2 - \rho_s h\omega^2 + \frac{K_r}{L}\left(\frac{\mu + 2(1)\pi}{L}\right)^2,$$

$$D2 = \frac{K_s}{R^2} n + \frac{D_s(1-\mu_s)}{R^2}\left(\frac{\mu + 2(1)\pi}{L}\right)^2 + \frac{D_s}{R^4} n^3,$$

$$E2 = D_s\left(\frac{\mu + 2(-1)\pi}{L}\right)^4 + \frac{D_s}{R^2}\mu_s\left(\frac{\mu + 2(-1)\pi}{L}\right)^2 n^2 - \mathrm{j}\frac{K_s}{R}\mu_s\left(\frac{\mu + 2(-1)\pi}{L}\right),$$

$$F2 = -\frac{D_s}{R^2}\mu_s\left(\frac{\mu + 2(-1)\pi}{L}\right)^2 n + \frac{D_s(1-\mu_s)}{R^2}\left(\frac{\mu + 2(-1)\pi}{L}\right)^2 n - \frac{D_s}{R^4} n^3 + \frac{K_s}{R^2} n,$$

$$G2 = \frac{D_s\mu_s}{R^2}\left(\frac{\mu + 2(-1)\pi}{L}\right)^2 n^2 + \frac{2D_s(1-\mu_s)}{R^2}\left(\frac{\mu + 2(-1)\pi}{L}\right)^2 n^2 + \frac{D_s}{R^4} n^4 + \frac{K_s}{R^2} - \rho_s h\omega^2$$
$$- \frac{H_n^2(k_{1r}R)\rho_1\omega^2}{H_n^{2'}(k_{1r}R)k_{1r}} + \frac{H_n^1(k_{2r}R)\rho_2\omega^2}{H_n^{1'}(k_{2r}R)k_{2r}} + \left(\frac{K_t}{L} - \frac{\omega^2 M}{L}\right) + \frac{K_r}{L}\left(\frac{\mu + 2(-1)\pi}{L}\right)^2,$$

$$H2 = \left(\frac{K_t}{L} - \frac{\omega^2 M}{L}\right) + \frac{K_r}{L}\left(\frac{\mu + 2(0)\pi}{L}\right)\left(\frac{\mu + 2(-1)\pi}{L}\right),$$

$$I2 = \left(\frac{K_t}{L} - \frac{\omega^2 M}{L}\right) + \frac{K_r}{L}\left(\frac{\mu + 2(1)\pi}{L}\right)\left(\frac{\mu + 2(-1)\pi}{L}\right),$$

$$J2 = D_s\left(\frac{\mu + 2(0)\pi}{L}\right)^4 + \frac{D_s}{R^2}\mu_s\left(\frac{\mu + 2(0)\pi}{L}\right)^2 n^2 - \mathrm{j}\frac{K_s}{R}\mu_s\left(\frac{\mu + 2(0)\pi}{L}\right),$$

$$K2 = -\frac{D_s}{R^2}\mu_s\left(\frac{\mu + 2(0)\pi}{L}\right)^2 n + \frac{D_s(1-\mu_s)}{R^2}\left(\frac{\mu + 2(0)\pi}{L}\right)^2 n - \frac{D_s}{R^4} n^3 + \frac{K_s}{R^2} n,$$

$$L2 = \frac{D_s\mu_s}{R^2}\left(\frac{\mu + 2(0)\pi}{L}\right)^2 n^2 + \frac{2D_s(1-\mu_s)}{R^2}\left(\frac{\mu + 2(0)\pi}{L}\right)^2 n^2$$
$$+ \frac{D_s}{R^4} n^4 + \frac{K_s}{R^2} - \rho_s h\omega^2 - \frac{H_n^2(k_{1r}R)\rho_1\omega^2}{H_n^{2'}(k_{1r}R)k_{1r}} + \frac{H_n^1(k_{2r}R)\rho_2\omega^2}{H_n^{1'}(k_{2r}R)k_{2r}}$$
$$+ \left(\frac{K_t}{L} - \frac{\omega^2 M}{L}\right) + \frac{K_r}{L}\left(\frac{\mu + 2(-1)\pi}{L}\right)\left(\frac{\mu + 2(0)\pi}{L}\right),$$

$$M2 = \left(\frac{K_t}{L} - \frac{\omega^2 M}{L}\right) + \frac{K_r}{L}\left(\frac{\mu + 2(0)\pi}{L}\right)^2,\ N2 = \left(\frac{K_t}{L} - \frac{\omega^2 M}{L}\right) + \frac{K_r}{L}\left(\frac{\mu + 2(1)\pi}{L}\right)\left(\frac{\mu + 2(0)\pi}{L}\right),$$

$$O2 = p_0\left[\varepsilon_n(-\mathrm{j})^n \mathrm{J}_n(k_{1r}R) - \frac{\varepsilon_n(-\mathrm{j})^n H_n^2(k_{2r}R)\mathrm{J}_n'(k_{1r}R)k_{1r}}{H_n^{2'}(k_{1r}R)k_{1r}}\right],$$

$$P2 = D_s\left(\frac{\mu + 2(1)\pi}{L}\right)^4 + \frac{D_s}{R^2}\mu_s\left(\frac{\mu + 2(1)\pi}{L}\right)^2 n^2 - \mathrm{j}\frac{K_s}{R}\mu_s\left(\frac{\mu + 2(1)\pi}{L}\right),$$

$$Q2 = -\frac{D_s}{R^2}\mu_s\left(\frac{\mu + 2(1)\pi}{L}\right)^2 n + \frac{D_s(1-\mu_s)}{R^2}\left(\frac{\mu + 2(1)\pi}{L}\right)^2 n - \frac{D_s}{R^4} n^3 + \frac{K_s}{R^2} n,$$

$$R2 = \frac{D_s\mu_s}{R^2}\left(\frac{\mu + 2(1)\pi}{L}\right)^2 n^2 + \frac{2D_s(1-\mu_s)}{R^2}\left(\frac{\mu + 2(1)\pi}{L}\right)^2 n^2$$

$$+ \frac{D_s}{R^4}n^4 + \frac{K_s}{R^2} - \rho_s h\omega^2 - \frac{H_n^2(k_{1r}R)\rho_1\omega^2}{H_n^{2'}(k_{1r}R)k_{1r}} + \frac{H_n^1(k_{2r}R)\rho_2\omega^2}{H_n^{1'}(k_{2r}R)k_{2r}}$$

$$+ \frac{K_t}{L} - \frac{\omega^2 M}{L} + \frac{K_r}{L}\left(\frac{\mu + 2(-1)\pi}{L}\right)\left(\frac{\mu + 2(1)\pi}{L}\right),$$

$$S2 = \frac{K_t}{L} - \frac{\omega^2 M}{L} + \frac{K_r}{L}\left(\frac{\mu + 2(0)\pi}{L}\right)\left(\frac{\mu + 2(1)\pi}{L}\right),$$

$$T2 = \frac{K_t}{L} - \frac{\omega^2 M}{L} + \frac{K_r}{L}\left(\frac{\mu + 2(1)\pi}{L}\right)^2.$$

As shown in equations (1)–(3) and (5)–(7), the solutions are obtained in a double series of the circumferential modes and space harmonic modes. The maximum space harmonics of 5 (i.e., $m = -5$–5) provided converged results for each n in this case, therefore this was adopted for all studies in this work. Then, the maximum number of the circumferential mode n was decided on after checking the convergence trend of the solution as the maximum n changes.

3. CALCULATION OF TRANSMISSION LOSS

The transmitted sound power per unit length of the shell in the interior cavity can be defined as

$$W^T = \frac{1}{2}\mathrm{Re}\left\{\int_0^{2\pi} p_2^T\, \partial/\partial t\,(w_1)^*\, R\, \mathrm{d}\theta\right\}, \quad \text{where } r = R. \tag{33}$$

Substitution of appropriate equations for p_2^T and w_1 into equation (33) yields an expression for the components of W_n^T,

$$W_n^T = \frac{1}{2}\mathrm{Re}\left\{\sum_{m=-\infty}^{\infty}(p_{2nm}^T H_n^1(k_{2r}R)(\mathrm{j}\omega w_{1nm}^0)^*)\right\} \times \int_0^{2\pi}\cos^2[n\theta]R\,\mathrm{d}\theta, \text{ where } r = R, \tag{34}$$

where $\mathrm{Re}\{\cdot\}$ and the superscript * in equations (33) and (34) represent the real part and the complex conjugate of the argument respectively. And $\varepsilon_n = 1$ for $n = 0$ and $\varepsilon_n = 2$ for $n = 1, 2, 3, \ldots$. The transmitted sound power is defined as

$$W_n^T = \frac{\pi R}{2\varepsilon_n} \times \mathrm{Re}\left\{\sum_{m=-\infty}^{\infty} p_{2nm}^T \times H_n^1(k_{2r}R) \times (\mathrm{j}\omega w_{1nm}^0)^*\right\}. \tag{35}$$

The power transmission coefficient is defined by

$$\tau(\gamma) = \frac{\sum_{n=0}^{\infty} W_n^T}{W^I}, \tag{36}$$

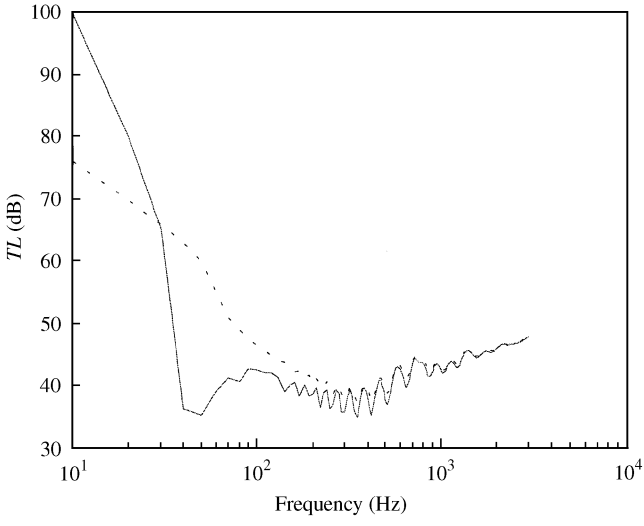

Figure 2. Comparison of the predicted averaged TLs between the stiffened and the unstiffened shells: ——, W/stiffener; ---------, W/O stiffener.

where W^I is the incident power with an angle γ per unit length of the shells in the axial direction,

$$W^I = \frac{\cos(\gamma) p_0^2}{\rho_1 c_1} \times 2R. \tag{37}$$

Then, a closed form for the power transmission coefficient that is a function of the angle of incidence (γ) can be obtained by substituting equations (35) and (37) into equation (36) as follows:

$$\tau(\gamma) = \sum_{n=0}^{\infty} \frac{\mathrm{Re}\left\{\sum_{m=-\infty}^{\infty} p_{2nm}^T \times H_n^1(k_{2r}R) \times (\mathrm{j}\omega w_{1nm}^0)^*\right\} \times \rho_1 c_1 \pi}{4\varepsilon_n \cos(\gamma) p_0^2}. \tag{38}$$

To estimate the random incidence TL, the TL is computed at a particular angle of incidence. Then the TL averaged over all possible angles of incidence, $\bar{\tau}$, is found according to the Paris formula [41] as

$$\bar{\tau} = 2 \int_0^{\gamma_{lim}} \tau(\gamma) \sin\gamma \cos\gamma \, \mathrm{d}\gamma, \tag{39}$$

where γ_{lim} is the limiting angle above which it is assumed that no sound is incident upon the shell. Calculated TL obviously depends on the choice of the angle of incidence in the analysis. This dependency can be removed by averaging TL over all possible incident angles as mentioned earlier. In the calculations to be presented in this paper, the power transmission coefficient has been calculated in steps of 2° from 0 to 80°, which was suggested by Mulholland *et al.* [42], and then equation (39) has been evaluated numerically. Finally, the averaged (or random incidence) TL is obtained as

$$TL_{avg} = 10 \log_{10}\left(\frac{1}{\bar{\tau}}\right). \tag{40}$$

Figure 2 shows the random incidence TLs of the unstiffened and stiffened shells, compared in a narrowband format when the mass effect of the stiffener is neglected. The simulation

TABLE 1

Dimensions of the cylindrical shell and simulation conditions

K_t (N/m)	$1{\cdot}0 \times 10^5$	ρ_s (kg/m^3)	7750	γ	$0 \sim 80^\circ$
K_r (N m/rad)	$1{\cdot}0 \times 10^3$	ρ_1 (kg/m^3)	1·21	L (mm)	100
E_s (Pa)	$1{\cdot}9 \times 10^{11}$	ρ_2 (kg/m^3)	1·21	ψ	1°
μ_s	0·3	c_1 (m/s)	343	R (m)	0·1
h (mm)	1·0	c_2 (m/s)	343	η_s	0·1
M (kg)	0	$\omega/2\pi$ (Hz)	$10 \sim 3000$	—	—

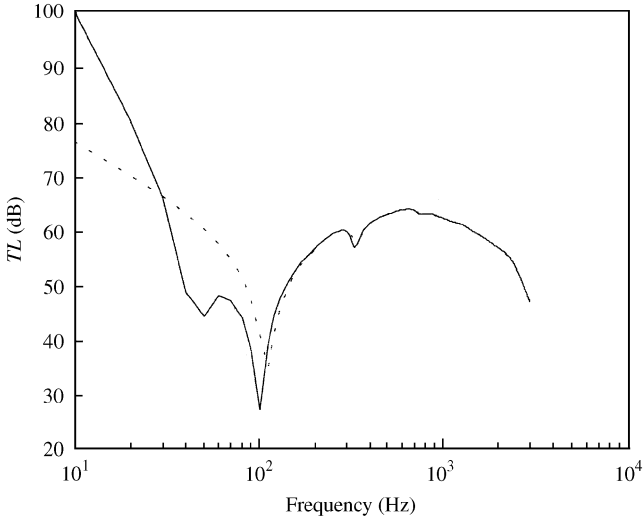

Figure 3. Comparison of the predicted TLs between the stiffened and the unstiffened shells on which a plane wave is incident with an angle of 45°: ——, W/stiffener; ---------, W/O stiffener.

conditions used to obtain Figure 2 are listed in Table 1. The unstiffened and stiffened shells for the single incident angle case for 45° are compared in terms of the TL in a narrowband format as shown in Figure 3 when the mass effect of the stiffener is also neglected. Figure 3 shows the sound transmission loss curve of the stiffened shell and of the unstiffened counterpart, in which the influence of stiffening can be clearly seen in the very low-frequency range. It is interesting to observe that the effect of the stiffening features is detrimental to the sound transmission characteristics of the stiffened shell in the frequencies ranging from 20 to 100 Hz when compared with an unstiffened shell. It can be qualitatively explained by the fact that free waves having wave number components of supersonic phase velocity can propagate at frequencies below the unstiffened shell critical frequency; these components may cause the shell to be exited in a coincidental manner by incident sound waves at

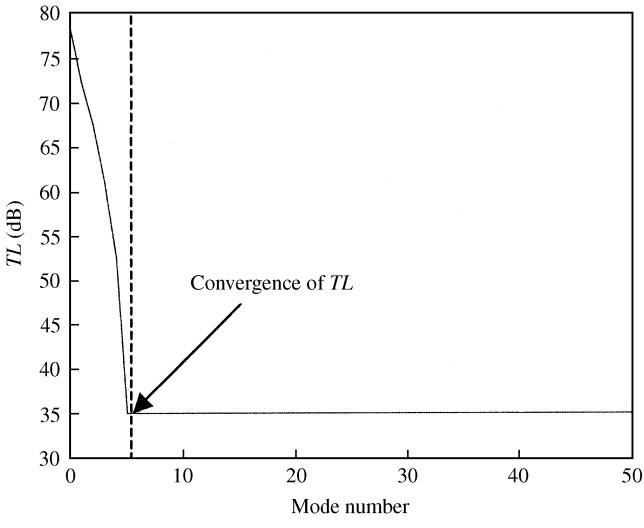

Figure 4. Coefficient covergence diagram for the cylindrical shell ($R = 0{\cdot}1$ m, $t = 1{\cdot}0$ mm) at 3000 Hz.

frequencies below critical. In practice, the effect on sound transmission is as though the critical frequency had been lowered by one or two octaves, the degree of change being dependent upon the phase attenuation coefficient, spacing and stiffness (translational and rotational) of the stiffeners [43].

4. CONVERGENCE OF THE SOLUTION

As one can see in equations (1)–(3) and (6)–(7), the solutions are obtained in series forms, which requires that enough terms have to be used in the calculation to ensure the solutions to converge. Once the solution converges at a given frequency, it can be assumed to converge in all frequencies lower than that, because more terms are necessary to be used in the calculation for a higher frequency. Therefore, the necessary number of circumferential modes has to be determined at the highest frequency of interest. A simple algorithm can be used to ensure the convergence of the solution in that the TL is calculated at the highest frequency of interest, adding one term at a time. When the TLs calculated at two successive calculations are within a pre-set error bound (0·01 dB in this work), the solution is considered to have converged. The number of modes found in this way is used to calculate TL at all other frequencies below this highest frequency of interest.

Figure 4 shows the calculated TL as the number of circumferential modes included (n) increases, while the number of space harmonics is fixed as 11 ($p = -5$–5) at the driving frequency of 3000 Hz. The same data shown in Table 1 are used for the stiffened shell but the incidence angle θ taken as 45°. From the figure, it is known that at least six circumferential modes ($n = 0$–5) have to be used to obtain a converged solution at 3000 Hz. This leads to a 66 term solution because 11 space harmonics and six circumferential modes are used. The necessary number of terms will have to be determined by considering the highest frequency of interest and the structural modes.

5. PARAMETER STUDIES

Studies of important design parameters are conducted for the stiffened shell with the same specifications listed in Table 1. TLs calculated for three different incident angles (30°, 45°,

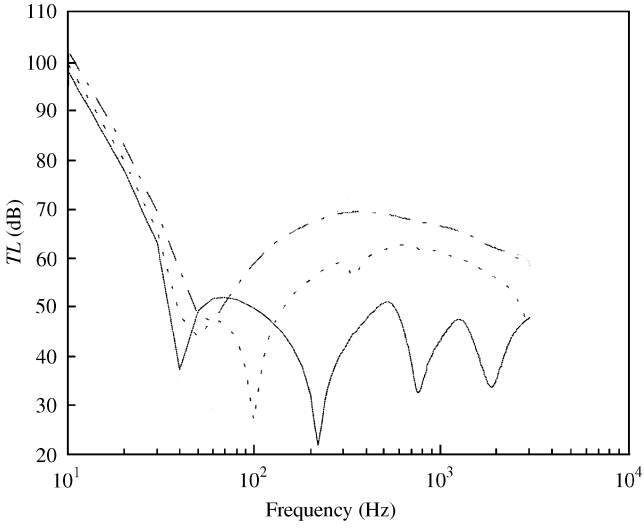

Figure 5. TL curves for the stiffened shell with respect to the incidence angle: ——, 30°; ---------, 45°; – · – · –, 60°.

60°) are shown in Figure 5, which indicate that the transmitted power slightly decreases (TL increases) with increasing incidence angle γ. Because the qualitative aspect of the solution does not change for different angles, the incident angle of 45° is used for all subsequent calculations, which reduces the related computation time substantially compared to the random incidence case.

5.1. PARAMETERS RELATED TO MODELLING

5.1.1. *Phase attenuation coefficient and shell loss factor*

As shown in Figure 6, the TL of the stiffened shell increases if the phase attenuation coefficient is increased, especially in the frequency range below 200 Hz. The attenuation coefficient seems to have little effect on the TL of the stiffened shell above 200 Hz.

A comparison of the TLs of the stiffened shells obtained for three different loss factors for the stiffened shell and zero loss factor for the unstiffened shell is shown in Figure 7. The figure shows that the loss factor plays an important role at every dip of the TL curve over the frequency range. From the figure, it is concluded that a damping treatment such as a coating will not give rise to enhancement of the TL to a significant extent as different from the stiffened panel [43]. It is also inferred that the increase of the loss factor would not be a solution to resolve the low TL characteristics in the low-frequency range of the stiffened shell as shown in Figure 7. Both the attenuation coefficient and loss factor are typically small, it is considered that arbitrary small values may be used. In the subsequent study, $\psi = 1^\circ$ as the phase attenuation coefficient angle and $\eta_s = 0{\cdot}1$ as the shell loss factor are used in this work.

5.1.2. *Stiffener mass effects*

TLs calculated for four different stiffener masses, which are 0, 10, 100, and 200% of the mass of the shell of one period of the stiffened shell, are plotted in Figure 8. The range of the parameter was taken intentionally to be very wide to observe the effect. There is no

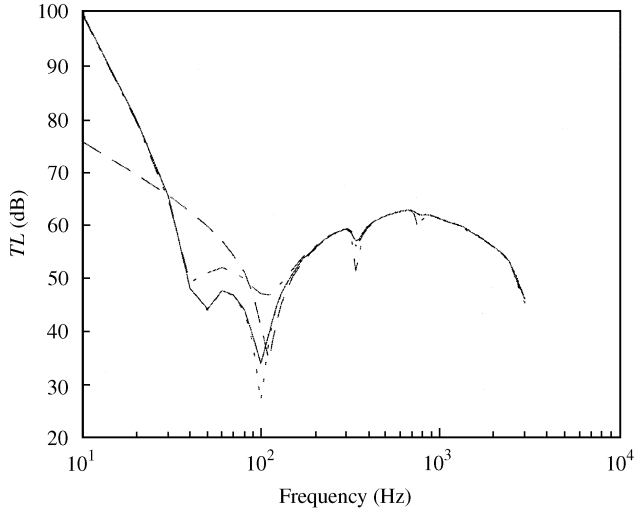

Figure 6. TL curves for the stiffened shell with respect to phase attenuation: ——, $\psi = 0°$; ---------, $\psi = 1°$; –·–·–, $\psi = 10°$; – – –, W/O stiffener.

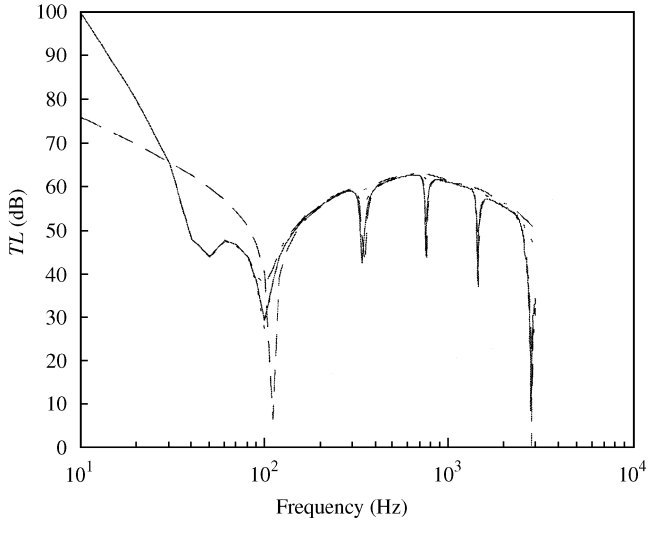

Figure 7. TL curves for the stiffened shell with respect to loss factor: ——, $\eta = 0$; ---------, $\eta = 0{\cdot}1$; –·–·–, $\eta = 0{\cdot}2$; – – –, W/O stiffener ($\eta = 0$).

significant difference in the TL curves between the 0 and 10% cases; 10% will be a very large stiffener mass in relation to the shell mass in practice. Hence, it can be concluded that the mass effect of the stiffener will not have to be considered in the analysis.

5.2. STUDY OF DESIGN PARAMETERS

5.2.1. *Materials*

Figure 9 shows the TL curves obtained for systems of different materials. Materials chosen for the comparison are steel, aluminum and brass as shown in Table 2. The figure

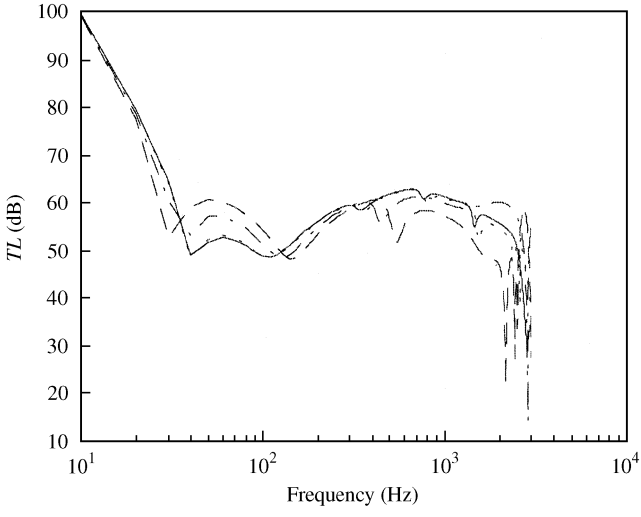

Figure 8. TL curves for the stiffened shell with respect to stiffener mass: ——, 0%; ---------, 10%; – · – · –, 100%; – – – -, 200%.

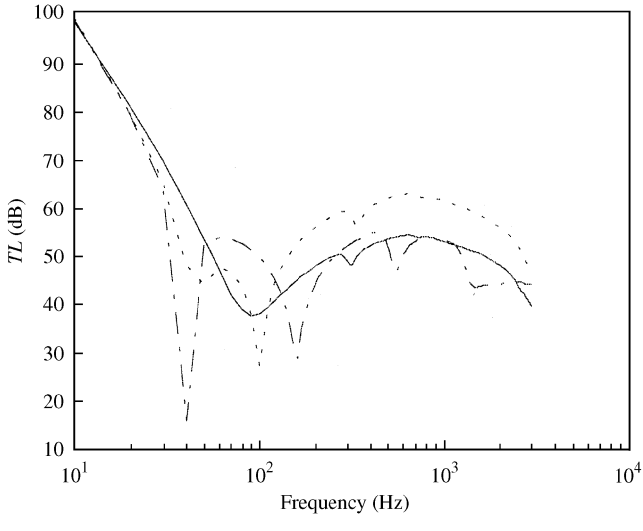

Figure 9. TL curves for the stiffened shell with respect to shell material: ——, aluminum; ---------, steel; – · – · –, brass.

shows that the steel is the most effective above 100 Hz, as expected because the stiffness of the steel is the largest. The figure also shows that aluminum, which has the lowest stiffness and density, is the least effective in the frequency range above 100 Hz, which is again as expected. Such a comparison may be used in practical design situations.

5.2.2. *Shell thickness*

As is seen in Figure 10, changing the thickness has a broadband effect on TL over the entire range of the frequency. In general, TL increases by 6 dB as the thickness doubles except in the very low-frequency range, which is well anticipated. In the low-frequency

TABLE 2

Material properties of the stiffened shell

	Steel	Aluminum	Brass
Density (ρ:kg/m^3)	7750	2700	8500
Young's modulus (E: Pa)	$1{\cdot}9 \times 10^{11}$	$0{\cdot}71 \times 10^{11}$	$1{\cdot}04 \times 10^{11}$
The Poisson ratio (v)	0·3	0·33	0·37

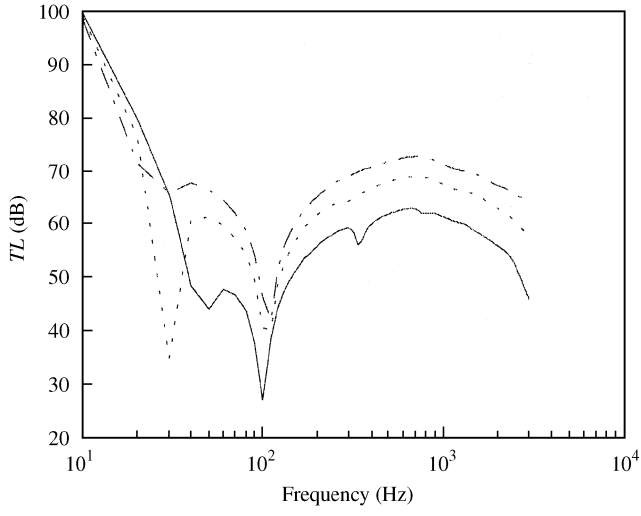

Figure 10. TL curves for the stiffened shell with respect to shell thickness: ——, $t = 1$ mm; ---------, $t = 2$ mm; –·–·–, $t = 3$ mm.

range, the reduction is lower than 6 dB because it is controlled more by the membrane stiffness. In a practical situation, when the shell has to be designed only as thick as necessary because of the weight constraint, this type of analysis will be very useful. For example, if a target TL is known from the consideration of the noise level, a proper thickness of the shell may be calculated correspondingly.

5.2.3. *Stiffener spacing*

As shown in Figure 11, smaller stiffener spacing has a much higher effect in the low-frequency range. As the stiffener spacing increases, the TL of the stiffened shell decreases especially in the low-frequency range, and eventually becomes close to that of the unstiffened shell as shown in Figure 11.

5.2.4. *Stiffness of the stiffener*

The effect of a larger stiffener is also more beneficial in the low-frequency range as shown in Figure 12. It is also interesting that an increase of the stiffener size does not contribute to

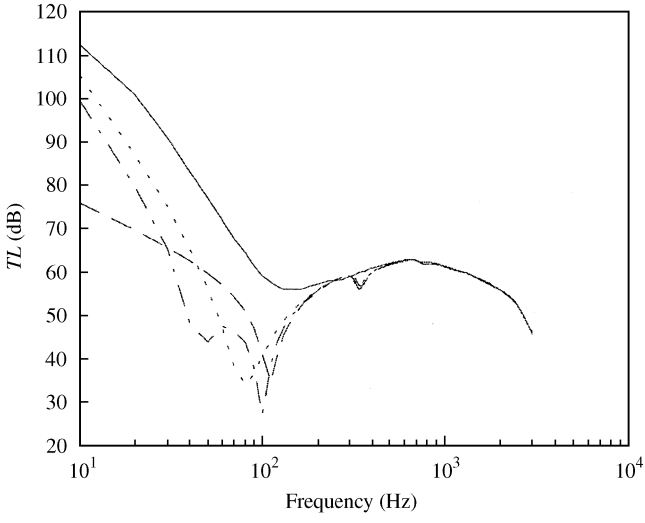

Figure 11. TL curves for the stiffened shell with respect to stiffener spacing: ——, $L = 10$ mm; ---------, $L = 50$ mm; –·–·–, $L = 100$ mm; – – –, W/O stiffener.

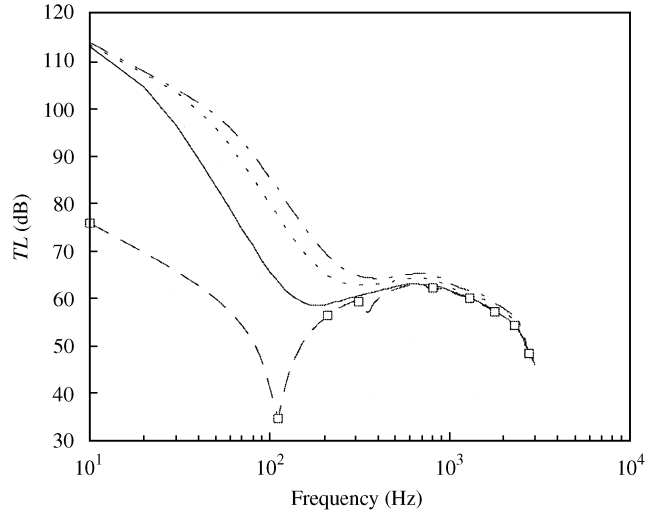

Figure 12. TL curves for the stiffened shell with respect to translational stiffness of the stiffener: —□—, $K_t = 0$ N/m; ——, $K_t = 2{\cdot}0 \times 10^6$ N/m; ---------, $K_t = 1{\cdot}0 \times 10^7$ N/m; –·–·, $K_t = 2{\cdot}0 \times 10^7$ N/m.

higher TLs until the stiffener size reaches a certain value ($K_t = 2 \times 10^7$ N/m in this case). This may be explained by considering that the effect of the increase of the translational stiffness becomes saturated after it exceeds the value that is sufficient to make the spring virtually a fixed support.

6. CONCLUSIONS

Solutions for the vibro-acoustic responses of a periodically stiffened cylindrical shell of infinite length are obtained analytically for the purpose of studying sound transmission

characteristics of stiffened shells. The system equation is derived by applying the virtual energy method. Love's equations are used to describe the shell motion, and the coupling effects between the shell and stiffener, and the shell and acoustic media are fully considered in the modelling. The motion of the shell and the reflected and transmitted waves induced by an incident plane wave are expanded in terms of the space harmonics in the solution procedure, which was developed by Mead *et al.* [1–3]. Because the solution is obtained as a truncated series, a convergence checking scheme is built into the solution procedure to include enough modes to obtain converged solutions. It is considered to be the first exact solution obtained for the sound transmission through stiffened cylindrical shells, which considers the full coupling effects between the structure and the acoustic media. Using the solutions represented in the transmission losses, characteristics of the system are studied to understand the effects of important modelling and design parameters and also to demonstrate the practical application of the analysis.

ACKNOWLEDGMENT

The authors acknowledge the financial support by ArvinMeritor Industries related to this work.

REFERENCES

1. D. J. MEAD *Journal of Sound and Vibration* **11**, 181–197. Free wave propagation in periodically supported, infinite beams.
2. D. J. MEAD and K. K. PUJARA 1971 *Journal of Sound and Vibration* **14**, 525–541. Space-harmonic analysis of periodically supported beams: response to convected random loading.
3. D. J. MEAD 1996 *Journal of Sound and Vibration* **190**, 495–524. Wave propagation in continuous periodic structures: research contributions from Southampton, 1964–1995.
4. Y. K. LIN 1960 *Journal of Applied Mechanics* **27**, 669. Free vibrations of continuous skin stringer panels.
5. C. A. MERCER 1965 *Journal of Sound and Vibration* **2**, 293. Response of a multi-supported beam to a random pressure.
6. M. HECKL 1964 *Journal of Acoustical Society of America* **36**, 1335. Investigations on the vibrations of grillages and other simple beam structures.
7. D. J. MEAD and E. M. WILBY 1971 *University of Southampton Report*. Forced vibration of periodically-supported beams subjected to convected, homogeneous pressure fields.
8. G. P. MATHUR, B. N. TRAN, J. S. BOLTON and N.-M. SHIAU 1992 *Proceedings of* 14*th DGLR/AIAA Aeroacoustical Conference*, 102–105. Sound transmission through stiffened double-panel structures lined with elastic porous materials.
9. W. DESMET and P. SAS 1995 *Proceedings of First Joint CEAS/AIAA Aeroacoustical Conference* (16*th AIAA Aeroacoustics Conference*), Vol. AIAA-95-043, 311–320. Sound transmission of finite double-panel partitions with sound absorbing material and panel stiffeners.
10. S. MUKHERJEE and S. PARTHAN 1995 *Journal of Sound and Vibration* **186**, 71–86. Wave propagation in one-dimensional multi-bay periodically supported panels under supersonic fluid flow.
11. Z. MECITOĞLU and M. C. DÖKMECI 1990 *Proceedings of the* 17*th Congress of the International Council of the Aeronautical Sciences*, Vol. 1, *AIAA*, *Washington*, *DC*, 986–993. Vibration analysis of stiffened circular cylindrical thin shells.
12. Z. MECITOĞLU and M. C. DÖKMECI 1990 *American Institute of Aeronautics and Astronautics Journal* **30**, *Technical Notes*, 848–850. Free vibration of a thin, stiffened, cylindrical shallow shell.
13. Z. MECITOĞLU 1996 *Journal of Sound and Vibration* **197**, 191–206. Vibration characteristics of a stiffened conical shell.
14. D. M. EGLE and J. L. SEWALL 1968 *American Institute of Aeronautics and Astronautics Journal* **6**, 518–526. An analysis of free vibration of orthogonally stiffened cylindrical shells with stiffeners treated as discrete elements.

15. D. BUSHNELL 1973 *American Institute of Aeronautics and Astronautics Journal* **11**, 1283–1291. Evaluation of various analytical models for buckling and vibration of stiffened shells.
16. D. J. MEAD and N. S. BARDELL 1987 *Journal of Sound and Vibration* **115**, 499–520. Free vibration of a thin cylindrical shell with periodic circumferential stiffeners.
17. B. A. J. MUSTAFA and R. ALI 1987 *Journal of Sound and Vibration* **113**, 317–327. Prediction of natural frequency of vibration of stiffened curved panels.
18. B. A. J. MUSTAFA and R. ALI 1989 *Computers and Structures* **32**, 355–363. An energy method for free vibration analysis of stiffened circular cylindrical shells.
19. B. SIVASUBRAMONIAN, G. V. RAO and A. KRISHNA 1999 *Journal of Sound and Vibration* **226**, 41–45. Free vibration of longitudinally stiffened curved panels with cutout.
20. K. Y. LAM and L. HUA 1999 *Journal of Sound and Vibration* **223**, 171–195. Influence of boundary conditions on the frequency characteristics of a rotating truncated circular conical shell.
21. Š. MARKUŠ and D. J. MEAD 1995 *Journal of Sound and Vibration* **181**, 127–147. Axisymmetric and asymmetric wave motion in orthotropic cylinders.
22. Š. MARKUŠ and D. J. MEAD 1995 *Journal of Sound and Vibration* **181**, 149–167. Wave motion in a three-layered, orthotropic–isotropic–orthotropic, composite shell.
23. P. W. SMITH JR 1957 *Journal of Acoustical Society of America* **29**, 712–729. Sound transmission through thin cylindrical shells.
24. P. WHITE 1966 *Journal of Acoustical Society of America* **40**, 1124–1130. Sound transmission through a finite, closed, cylindrical shell.
25. L. R. KOVAL 1976 *Journal of Sound and Vibration* **48**, 265–275. On sound transmission into a thin cylindrical shell under flight conditions.
26. L. R. KOVAL 1977 *American Institute of Aeronautics and Astronautics Journal* **15**, 899–900. Effects of stiffening on sound transmission into a cylindrical shell in flight.
27. L. R. KOVAL 1979 *Journal of Sound and Vibration* **63**, 51–59. On sound transmission into an orthotropic shell.
28. L. R. KOVAL 1980 *Journal of Sound and Vibration* **71**, 523–530. Sound transmission into a laminated composite cylindrical shell.
29. A BLAISE, C. LESUER, M. GOTTELAND and M. BARBE 1991 *Journal of Sound and Vibration* **150**, 233–243. On sound transmission into an orthotropic infinite shell: comparison with Koval's results and understanding of phenomena.
30. Y. Y. TANG, J. H. ROBINSON and R. J. SILCOX 1996 34th *AIAA Aerospace Science Meeting and Exhibit* (*AIAA-96-0877*), 1–10. Sound transmission through a cylindrical sandwich shell with honeycomb core.
31. Y. Y. TANG, R. J. SILCOX and J. H. ROBINSON 1996 *Proceedings of the* 14*th International Modal Analysis Conference*, *Japan*, 1488–1492. Sound transmission through two concentric-cylindrical-sandwich shells.
32. F. P. GROOTEMAN, D. BOER and H. SCHIPPERS 1995 *CEAA/AIAA* 1*st Joint Aeroacoustic Conference*, 1049–1053. Vibro-acoustic analysis of double wall structures.
33. J. H. LEE and J. KIM *Journal of Sound and Vibration*. Exact calculation of the transmission loss of the thin shell enclosing cylindrical cavity (under review).
34. J. H. LEE and J. KIM *Journal of Sound and Vibration*. Analysis and measurement of sound transmission through a double-walled cylindrical shell (accepted).
35. J. H. LEE and J. KIM 2001 *Journal of Acoustic Society of America* **110**, 2282–2294. A new simplified modeling method of sound transmission through double panel with absorptive porous core.
36. J. H. LEE and J. KIM 2000 *Proceeding of International Compressor Conference at Purdue University*, 933–940. Sound transmission through cylindrical shell of hermetic compressors.
37. W. SOEDEL 1993 *Vibrations of Shells and Plates*. New York: Marcel Dekker, Inc.
38. M. MORSE and K. UNO INGARD 1968 *Theoretical Acoustics*. New York: McGraw-Hill.
39. L. E. KINSLER, A. R. FREY, A. B. COPPENS and J. V. SANDERS 1982 *Fundamentals of Acoustics*. New York: John Wiley & Sons, Inc.
40. C. M. HECKL and E. E. UNGAR 1973 *Structure-Borne Sound*. Berlin: Springer-Verlag.
41. D. PIERCE 1981 *Acoustics*. New York: McGraw-Hill.
42. K. A. MULHOLLAND, H. D. PARBROOK and A. CUMMINGS 1967 *Journal of Sound and Vibration* **6**, 324–334. The transmission loss of double panels.
43. F. FAHY 2000 *Sound and Structural Vibration*. New York: Academic Press.